Spin Splitting of Single 0D Impurity States in Semiconductor Heterostructure Quantum Wells

M. R. Deshpande, J. W. Sleight,* M. A. Reed, and R. G. Wheeler
Departments of Physics, Applied Physics, and Electrical Engineering, Yale University, P.O. Box 208120, New Haven, Connecticut 06520

R. J. Matyi†
Central Research Laboratories, Texas Instruments Incorporated, Dallas, Texas 75265
(Received 2 June 1995)

Zeeman splitting of the ground state of single impurities in the quantum well of a resonant tunneling heterostructure is reported. We determine the absolute magnitude of the effective magnetic spin splitting factor $g_{\perp}^{*}$ for a single impurity in a 44 Å $Al_{0.27}Ga_{0.73}As/GaAs/Al_{0.27}Ga_{0.73}As$ quantum well to be 0.28 $\pm$ 0.02. This system also allows for independent measurement of the electron tunneling rates through the two potential barriers and estimation of the occupation probability of the impurity state in the quantum well.

PACS numbers: 73.20.Hb, 71.55.Eq, 73.20.Dx, 73.40.Gk

The experimental realization of granular electronic systems, such as low dimensional semiconductor and ultrasmall metallic systems, has focused attention on the basic physical properties of discrete systems. Especially intriguing are the semiconductor quantum dot [1–5] and the physically similar localized impurity state tunneling systems [6–10]. The latter provides a unique laboratory for the study of a single impurity. We present here the first observation of Zeeman spin splitting of a single semiconductor impurity, studied by tunneling transport. The measured g^* factor provides an important test of the band theory of confined semiconductor systems, and our method is particularly important for well widths less than 50 Å where other methods are less precise [11–13].

Isolated donor impurities in the quantum well regions of large area resonant tunneling structures form localized ($\sim$100 Å) hydrogenic states bound to the quantum eigenstates. Figure 1 illustrates a band diagram of the structure used in this study with one impurity state in the well schematically noted. In an applied bias when the impurity state aligns with the emitter Fermi level, the current exhibits a steplike increase. In general, there may be multiple impurities giving rise to multiple, overlapping steps in the current-voltage [$I(V)$] characteristics. An appropriately dilute, unintentional doping concentration gives rise to isolated, uncorrelated impurities, allowing measurement of a single one. In a magnetic field the spin degeneracy of the impurity ground state is broken, resulting in a splitting of the current step in the $I(V)$ characteristics. The magnitude of the spin g^* factor can be determined from the voltage difference between the two fragments of the spin-split step. The current magnitudes of the two fragments enable us, for the first time, to independently determine the electron tunneling rates through the two potential barriers in a sequential tunneling picture [4,14].

The nominally symmetric resonant tunneling heterostructure is grown by molecular beam epitaxy (MBE) on a Si-doped GaAs(100) substrate [15]. The epitaxial layers consist of a 1.8×10^{18} cm^{-3} Si doped GaAs contact, a 15 nm undoped GaAs spacer layer, a 8.5 nm undoped $Al_{0.27}Ga_{0.73}As$ bottom barrier, a 4.4 nm undoped GaAs quantum well, a 8.5 nm undoped $Al_{0.27}Ga_{0.73}As$ top barrier, a 15 nm undoped GaAs spacer layer, and a 1.8×10^{18} cm^{-3} Si doped GaAs top contact. Square mesas with lateral dimensions from 2 to 64 μm are fabricated using standard photolithography techniques. Two terminal $I(V)$ characteristics are measured in a dilution refrigerator with a base temperature of 50 mK.

Figure 2 shows the $I(V)$ characteristics for a typical device (64 μm^2, 1.4 K) showing the main quantum well resonance peaks (top). Magnification of the current in the prethreshold region (bottom) shows two sharp current steps for both forward and reverse bias directions. This step structure is observed to be sample specific, but for a given sample it is exactly reproducible from one voltage sweep to another and independent of the voltage sweep direction. The steps are reproduced even after thermal cycling of the sample, except for slight threshold

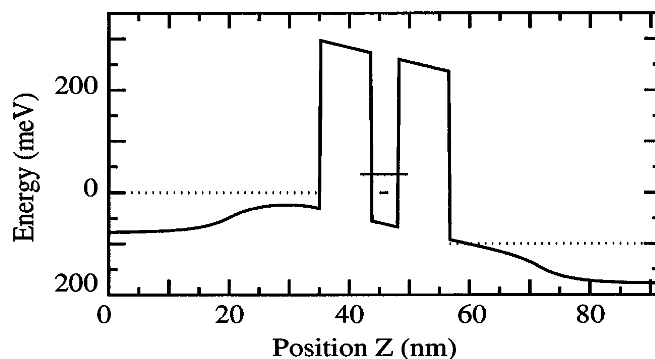

FIG. 1. Model conduction band diagram of the device, at an applied bias of 100 mV, showing the quantum eigenstate (long line) and a localized impurity state (short line) in the well. The dotted line represents the Fermi level in the leads.

0031-9007/96/76(8)/1328(4)$06.00
© 1996 The American Physical Society

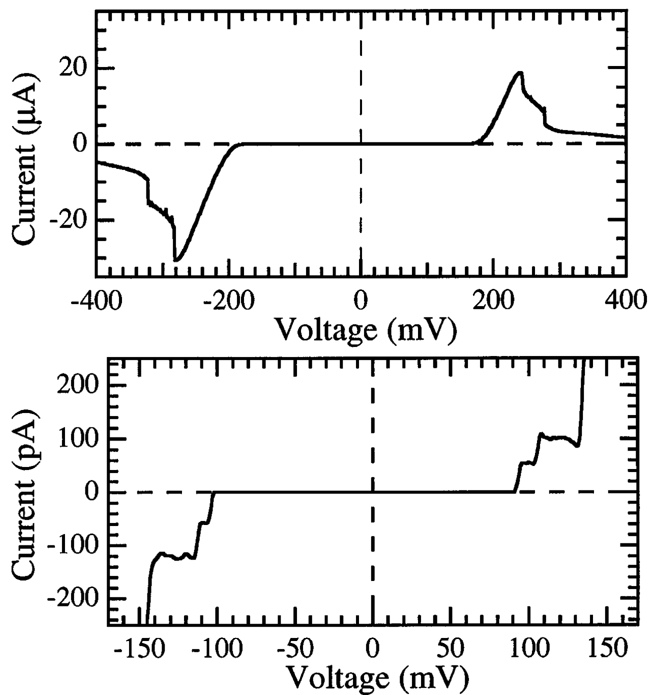

FIG. 2. $I(V)$ characteristics (zero magnetic field) at 1.4 K of the quantum well device showing the main resonance peaks (top). The magnified prethreshold region shows two steplike structures due to two isolated impurities (bottom).

voltage shifts (<1 mV). Similar steps are observed in other devices with different barrier thicknesses. The step current magnitudes are observed to be of the order of e/τ (e is the electronic charge and τ is the lifetime of the quantum well state as estimated from a band-profile model [9]). This suggests that the current steps are due to single electron tunneling through individual, zero dimensional states in the quantum well. Similar features have been observed and reported previously [6,7], and are attributed to tunneling through bound states of impurities in the quantum well.

Figure 3 shows an expanded view of the first current step edge at 50 mK for forward and reverse bias at 0 and at 9 T. The magnetic field is oriented perpendicular to the current direction (parallel to the heterointerfaces). At zero field, the ground state of the impurity is spin degenerate, leading to a single current step. Upon lifting of the degeneracy at finite fields, a splitting of the current step is observed [16]. Figure 4 shows the voltage separation between the corresponding two spin-split conductance peaks which increases linearly with the magnetic field strength as expected. Because of the finite widths of the conductance peaks, it is not possible to resolve the splitting for magnetic fields less than 5.5 T. The best fit line to the data (Fig. 4) closely intersects $\Delta V = 0$ at $B = 0$ and has a slope $g^*_\perp \mu_B/\alpha$, where μ_B is the Bohr magneton, $g^*_\perp$ is the effective gyromagnetic ratio of the impurity with the magnetic field perpendicular to the growth direction of the quantum well, and α is the voltage to energy conversion factor [4,5,8].

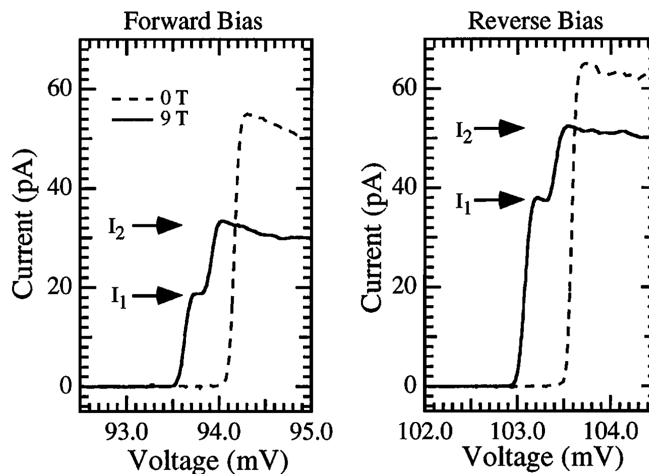

FIG. 3. $I(V)$ characteristics at 50 mK of the first current step edge in forward bias (left) and reverse bias (right) at 0 T (dashed line) and 9 T (solid line). I_1 and I_2 mark the current values at 9 T as shown. I_1 gives the current of the first fragment while I_2 is the net current of both fragments of the split step edge.

The current through a localized impurity state in the quantum well, at bias V and temperature T, depends upon the density of occupied electronic states in the emitter at the same energy as the impurity state, which is proportional to the Fermi distribution function f. The current plateau edges exhibit characteristic Fermi level thermal broadening. We can express the current as

$$I(V,T) = 2I_{\text{th}} f(V,T) = \frac{2I_{\text{th}}}{1 + \exp[\alpha e(V_{\text{th}} - V)/kT]}, \quad (1)$$

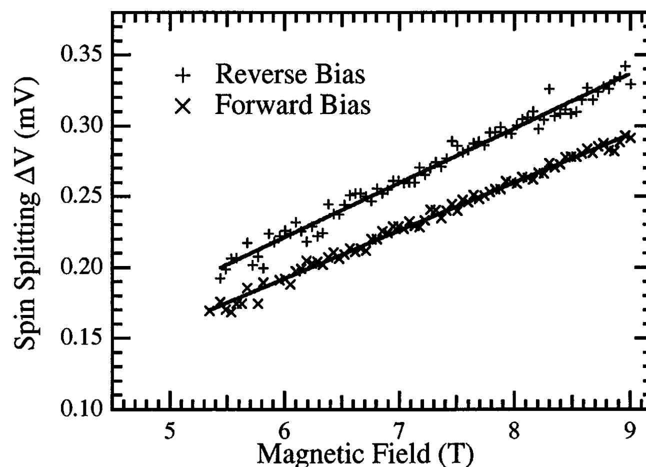

FIG. 4. The experimental spin splitting versus magnetic field perpendicular to current for the first current step in forward and reverse bias at 50 mK. The solid lines are linear fits to the data.

where e is the electron charge, k is Boltzmann's constant, and $V_{\rm th}$ and $I_{\rm th}$ are the threshold voltage and current at the observed common intersection point of the various $I(V)$ curves at different temperatures. The only free parameter α is determined from a fit of the above Fermi function to the $I(V)$ traces at zero magnetic field. The fits are done for data taken at eight different temperatures, from 0.8 to 5 K, and the average value of α along with the rms error is reported. We obtain $\alpha = 0.48 \pm 0.02$ for forward bias and 0.42 ± 0.02 for reverse bias. The fits are done for the region $V \leq V_{\rm th}$ when the current is small and not affected by the occupancy of the impurity state.

From these values of α and the measured slope of the spin splitting versus magnetic field, the absolute magnitude of the spin $g_\perp^*$ value of the impurities is determined. The two steps in Fig. 2 correspond to two separate impurities. We obtain for the lower bias, first impurity, $g_\perp^* = (0.28 \pm 0.02, 0.28 \pm 0.02)$ (for forward and reverse bias, respectively) and for the higher bias, second impurity, $g_\perp^* = (0.28 \pm 0.02, 0.27 \pm 0.02)$.

The g^* value of electrons in bulk GaAs (-0.44) is different from the free electron value (+2) due to the spin orbit interaction in the valence band and its effect on the conduction band as analyzed using $\vec{k} \cdot \vec{p}$ theory. In confined quantum well regions, it changes further and also becomes anisotropic. This is partly due to the change in the electron and hole energies due to confinement, and partly due to the electron wave-function penetration in the barrier material where the electron has a higher g^* value (+0.39). g^* is theoretically predicted to be a strong function of the quantum well width and changes from the bulk value of -0.44 to greater than +0.4 for well widths less than 30 Å [11]. Our measurement is consistent with this prediction and with recent experimental results [12,13] (assuming here that the sign of g^* is positive).

Because of the 3D nature of the emitter, at any given energy electrons of both spin orientations are available for tunneling (even with applied magnetic field). Figure 5 shows thermal broadening of the first current step edge at 9 T. Separate Fermi broadening of the two fragments indicates that in both cases electrons involved in tunneling are the Fermi electrons in the emitter. The observed experimental voltage difference is thus entirely due to the spin splitting of the impurity state, and is not affected by the g^* factor of the electrons in the emitter [17]. We also note that electron-electron interactions will not alter the relative energy of the two spin states and thus the measured g^* factor. Coulomb interaction between the tunneling electron and the electrons in the emitter causes a rise in the step current near the threshold at low temperatures, which is observed (as first reported by Geim *et al.* [8]), but it should not affect the energy separation of the two spin states.

Analysis of the tunneling current through the spin-split system yields additional information about the tunneling process. Recalling Fig. 3, the two fragments of the spin-split step at 9 T are observed *not* to have the same current magnitude ($I_2 - I_1 \neq I_1$). This difference is more prominent in reverse bias. To analyze this, we define Γ_b and Γ_t to be the tunneling rates for an electron to tunnel through the bottom and the top (referred to growth direction) potential barriers, respectively, of the double barrier heterostructure. We also define $\Gamma_{\rm cl}$ and $\Gamma_{\rm em}$ to be the electron tunneling rates through the collector (downstream) and emitter (upstream) (referred to electron flow direction) potential barriers. In forward bias, electron injection is through the top barrier into the quantum well ($\Gamma_{\rm em} \equiv \Gamma_t$, $\Gamma_{\rm cl} \equiv \Gamma_b$), while in reverse bias, electron injection is through the bottom barrier into the quantum well ($\Gamma_{\rm em} \equiv \Gamma_b$, $\Gamma_{\rm cl} \equiv \Gamma_t$). We also define p to be the occupation probability for an electron in a localized state in the quantum well. In the sequential tunneling picture, $p = f\Gamma_{\rm em}/(\Gamma_{\rm em} + \Gamma_{\rm cl})$. Since the spin splitting energy ($\Delta E \leq 150\ \mu$eV) is much smaller than the barrier potential energy ($\approx$300 meV), we assume that the tunneling rates are the same for electrons tunneling through spin up or spin down states. We also assume that the emitter electrons are not spin polarized, which is a good assumption since the Fermi energy ($\sim$40 meV) is much larger than the spin splitting energy even at 10 T.

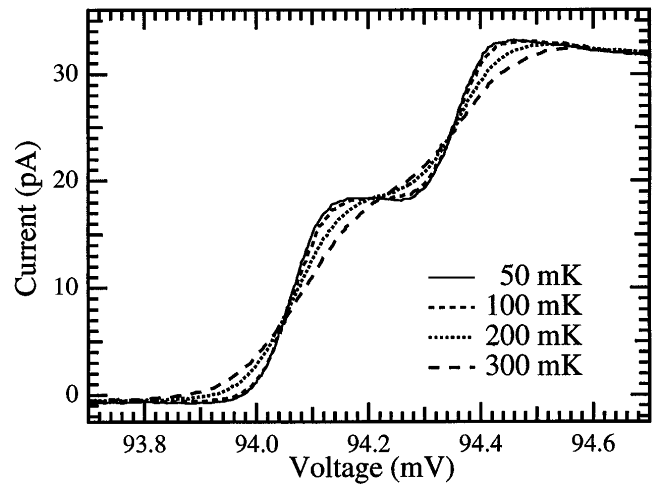

FIG. 5. $I(V)$ characteristics at 9 T showing the spin-split first current step edge in forward bias at temperatures ranging from 50 to 300 mK.

In high magnetic fields and at low temperatures, when the Fermi level is sharp (Fig. 5), we can adjust the bias to have the following two cases for a given impurity. At lower bias, only the lower energy spin state channel is active for conduction, and the current is given by

$$I_1 = pe\Gamma_{\rm cl}\,. \qquad (2)$$

At higher bias, the higher energy spin state channel is also active for conduction, and the current is given by

$$I_2 = p'e\Gamma_{\rm cl} = (2p - p^2)e\Gamma_{\rm cl}\,, \qquad (3)$$

where $p' = 2p - p^2$ is the probability of occupying either the lower or the higher state, but not both of

them. Both states cannot be occupied at the same time due to the large Coulomb energy required for another electron to simultaneously occupy the second state. For this system the single electron Coulomb charging energy ($U_C = e^2/2C$ where C is the effective capacitance of the double barrier device [3–5,18]) is much larger than the spin splitting energy ΔE.

In the extreme limits these equations indicate that for $\Gamma_{cl} \gg \Gamma_{em}$, $p \approx 0$ and $I_2 \approx 2I_1$ while for $\Gamma_{cl} \ll \Gamma_{em}$, $p \approx 1$ and $I_2 \approx I_1$. This qualitatively explains the behavior observed in Fig. 3. To get a quantitative understanding, we solve Eqs. (2) and (3), using I_1 and I_2, to determine p. For the first impurity at 9 T, $p = 0.21 \pm 0.01$ for forward bias and $p = 0.62 \pm 0.02$ for reverse bias. A high p value indicates that the electron tunneling rate through the collector (downstream) barrier (Γ_{cl}) is lower than that through the emitter (upstream) barrier (Γ_{em}) causing an accumulation in the well. A higher p value for reverse bias (as compared to forward bias) implies an asymmetry in the heterostructure growth, suggesting that the top barrier is slightly thicker than the bottom barrier. This is consistent with the difference in the measured α values, observed asymmetry in the $I(V)$ characteristics for this sample [the main resonance peak voltage and peak current values are higher for reverse bias as compared to forward bias (Fig. 2)], and is in agreement with previous characterization [15].

We can also obtain the absolute magnitude of the electron tunneling rates through the two potential barriers and study their dependence on the magnetic field perpendicular to current. For a reverse bias voltage of 103 mV Γ_{em} decreases from $(8.5 \pm 0.3) \times 10^8$ s^{-1} at 6 T to $(6.5 \pm 0.3) \times 10^8$ s^{-1} at 9 T as the field is increased. On the other hand, Γ_{cl} is approximately constant at $(4.0 \pm 0.3) \times 10^8$ s^{-1} in that field range. Similar values and trends are observed in forward bias. The suppression of Γ_{em} results in the observed plateau current suppression with magnetic field [19]. This indicates that the magnetic field affects the emitter-to-well tunneling process (Γ_{em}) more than it affects the well-to-collector tunneling process (Γ_{cl}). We therefore expect more current suppression when the current is emitter barrier limited than when it is collector barrier limited, which is observed (Fig. 3). For forward bias (thicker emitter) the current at 9 T is suppressed by a factor of 41% (as compared to 0 T), while the suppression is only 20% for reverse bias (thicker collector).

We have presented a $g_\perp^*$ measurement for a given epitaxial structure. This method can be used for a precise determination of g^* as a function of quantum well width and magnetic field orientation to compare to theory. This technique generalizes to other measurements of interest such as the $g^*(B)$ dependence, the investigation of magnetic impurities [20], different heterojunction material systems, and the determination of tunneling rates for band-gap engineered structures of interest.

We thank Professor D. E. Prober, Dr. M. Amman, and J. U. Nöckel for many useful discussions, C. L. Fernando and Professor W. R. Frensley for help with the modeling, and A. Mittal for experimental assistance. This work is supported by NSF Grants No. DMR-9112497 and No. DMR-9216121.

*Present address: Digital Semiconductor, Hudson, MA.
†Present address: Department of Materials Science and Engineering, University of Wisconsin, Madison, WI.

[1] M. A. Reed *et al.,* Phys. Rev. Lett. **60**, 535 (1988).
[2] S. Tarucha, Y. Hirayama, T. Saku, and T. Kimura, Phys. Rev. B **41**, 5459 (1990).
[3] M. Teowordt *et al.,* Phys. Rev. B **46**, 3948 (1992).
[4] B. Su, V. J. Goldman, and J. E. Cunningham, Phys. Rev. B **46**, 7644 (1992).
[5] J. W. Sleight *et al.,* Phys. Rev. B (to be published).
[6] M. W. Dellow *et al.,* Phys. Rev. Lett. **68**, 1754 (1992); J. W. Sakai *et al.,* Appl. Phys. Lett. **64**, 2563 (1994).
[7] M. R. Deshpande *et al.,* in *Proceedings of the IEEE/Cornell Conference on Advanced Concepts in High Speed Semiconductor Devices and Circuits, Ithaca, New York, 1993* (IEEE, New York, 1993), p. 177; M. R. Deshpande *et al.,* Semicond. Sci. Technol. **9**, 1919 (1994).
[8] A. K. Geim *et al.,* Phys. Rev. Lett. **72**, 2061 (1994).
[9] M. R. Deshpande *et al.,* in *Proceedings of the 22nd International Conference on the Physics of Semiconductors, Vancouver, Canada, 1994,* edited by D. J. Lockwood (World Scientific, Singapore, 1995), p. 1899.
[10] J. W. Sakai *et al.,* Solid-State Electron. **37**, 965 (1994).
[11] E. L. Ivchenko and A. A. Kiselev, Sov. Phys. Semicond. **26**, 827 (1992).
[12] M. J. Snelling *et al.,* Phys. Rev. B **44**, 11 345 (1991); M. J. Snelling *et al.,* Phys. Rev. B **45**, 3922 (1992).
[13] R. M. Hannak *et al.,* Solid State Commun. **93**, 313 (1995).
[14] We assume sequential tunneling because the barriers are thick (85 Å). S. Luryi, Appl. Phys. Lett. **47**, 490 (1985).
[15] M. A. Reed *et al.,* Appl. Phys. Lett. **54**, 1256 (1989).
[16] Splitting is also observed when the magnetic field is parallel to the current direction. We restrict this paper to the case of magnetic field perpendicular to current.
[17] If the Fermi energy in the emitter is small and weakly localized states are formed in the emitter, the g^* factor of these weakly localized states would have to be taken into account as reported by Sakai *et al.* [10].
[18] $C = (\epsilon_0 k \pi r_0^2)(d_t^{-1} + d_b^{-1})$, where k is the dielectric constant, d_t and d_b are the top and bottom barrier thicknesses, and r_0 is the radius of the lateral region affected by the localized impurity state in the quantum well. We take r_0 as the Bohr radius of hydrogenic impurities in GaAs (≈ 100 Å) and obtain $U_C \approx 9$ meV. Although taking r_0 as the Bohr radius is only an approximation, we obtain $U_C \geq \Delta E$ even for r_0 seven times larger.
[19] J. W. Sakai *et al.,* Phys. Rev. B **48**, 5664 (1993).
[20] V. I. Sugakov and S. A. Yatskevich, Sov. Tech. Phys. Lett. **18**, 134 (1992).